Journal of Crystal Growth 415 (2015) 78–83

Contents lists available at ScienceDirect

Journal of Crystal Growth

journal homepage: www.elsevier.com/locate/jcrysgro

Chemical vapor deposition of m-plane and c-plane InN nanowires on Si (100) substrate

Subrina Rafique, Lu Han, Hongping Zhao *

Department of Electrical Engineering and Computer Science, Case Western Reserve University, Cleveland, OH 44106, United States

ARTICLE INFO

Article history:
Received 3 September 2014
Received in revised form
16 December 2014
Accepted 31 December 2014
Communicated by J.M. Redwing
Available online 8 January 2015

Keywords:
A3. Chemical vapor deposition processes
A3. Vapor–liquid–solid
B1. InN nanowires
B1. Semiconductor III–V materials

ABSTRACT

In this paper, synthesis of indium nitride (InN) nanowires (NWs) by chemical vapor deposition (CVD) is studied. InN NWs were synthesized via a vapor–liquid–solid (VLS) growth mechanism using high purity indium foil and ammonia as the source materials, and nitrogen as carrier gas. The mixture of nonpolar m-plane oriented and polar c-plane oriented tapered InN NWs is observed grown on top of Si (100) substrate. Energy dispersive spectroscopy (EDS) showed that the tips of the NWs are primarily consisted of Au and the rest of the NWs are consisted of indium (In) and nitrogen (N). High resolution scanning electron microscopy (HRSEM) revealed that the InN NWs have both triangular and hexagonal cross sections. Transmission electron microscopy (TEM) diffraction pattern showed that the NWs are high quality single crystals having wurtzite crystal structure. High resolution transmission electron microscopy (HRTEM) showed the growth directions of the InN NWs with triangular cross section are along $\langle 10-10 \rangle$ nonpolar m-plane orientation and the InN NWs with hexagonal cross section are along $\langle 0001 \rangle$ polar c-plane orientation.

1. Introduction

III-nitride (Al-, Ga-, In, -N) semiconductors have been widely applied in electronic and optoelectronic devices including high power transistor [1], light-emitting diodes [2–4] and laser diodes [5–7]. Among the III-nitride compound semiconductors, InN has the narrowest direct bandgap of ~0.7–0.8 eV [8,9], large drift velocity at room temperature and low electron effective mass resulting in high mobility and saturation velocity [10–12]. However, InN remains the least studied material among the III-nitride compounds due to its low dissociation temperature and low nitrogen vapor pressure at that temperature which makes it difficult to synthesize. In addition, for the synthesis of InN thin films, suitable lattice-matched substrate is still lacking. The most commonly selected substrate is sapphire, for which the lattice mismatch is ~21% [13]. The use of GaN buffer layer on top of sapphire can reduce the lattice mismatch from ~21% to ~11% which is still large [13]. The structural and electrical quality of the InN thin film has not been improved significantly even after the use of GaN buffer layer. The lattice mismatch between InN and silicon (Si) is even larger (~35%). Thus, the growth of high quality InN thin film on Si substrate remains a great challenge [14,15].

Synthesis of one-dimensional nanowires (NWs) has been demonstrated on various substrates. Chemical vapor deposition (CVD) is a viable approach for growth of InN NWs. There are several reports on InN NWs synthesis using CVD approach [16–32]. Both vapor–solid (VS) [16–22] and vapor–liquid–solid (VLS) [23–27] growth mechanisms have been proposed to explain the synthesis of InN NWs. Different growth substrates such as Si [24,25,29], Si/SiO_2 [23,26], Al_2O_3 membrane [16], SiC [29], carbon cloth [27], amorphous quartz [30], polycrystalline AlN [30], sapphire [30], and GaN [28] have been used. Among all, Si substrate is more attractive due to its potential advantage to integrate the as-grown devices with the currently existing and developed IC technologies. Si substrates with different crystallographic orientations have been used by several groups to synthesize InN nanowires. Liang et al. reported the growth of InN nanowires on P type Si (100) substrate which grew along [110] direction [24]. Liu et al. reported the growth of $\langle 0-111 \rangle$ oriented InN nanowires on Si (100) substrate [25]. Sardar et al. synthesized InN nanowires on Si (100) substrate along the $\langle 101 \rangle$ direction [31]. On the other hand, when Si (111) substrate was used by Chang et al., they obtained InN nanowires with their c-axis oriented vertically to the substrate [32]. Both pure indium (In) and In_2O_3 have been used as group III precursor. Although widely used, In_2O_3 as the group III precursor has some disadvantages as it incorporates oxygen contamination into the synthesized InN which results in (1) the formation of oxygen–InN alloy or (2) the increased bandgap from the Burstein–Moss effect with oxygen serving as donor [33,34].

* Corresponding author.
E-mail address: hongping.zhao@case.edu (H. Zhao).

http://dx.doi.org/10.1016/j.jcrysgro.2014.12.039
0022-0248/

One great challenge associated with the NW growth is the control of its morphology, size uniformity and growth direction on various substrates. To achieve precise control of the growth direction, besides the NW growth condition, choice of substrate is very crucial. For successful heteroepitaxial growth of NWs, a match between the lattice constants of the NW and the substrate is indispensable and it also influences the NW growth direction strongly. Nanowires prefer to grow in the crystal direction which minimizes the total energy of the system. For NWs with cubic crystal structure, (111) plane has the lowest energy and thus the nanowires grow along the ⟨111⟩ direction [35]. But for heteroepitaxy of compound semiconductors, it is more difficult to control the growth direction precisely because of the lattice mismatch between the NW and the substrate. For NWs with wurtzite crystal structure, it is possible to choose a substrate with similar crystal structure to closely match either of the lattice constants (a or c). Kuykendall et al. demonstrated the control of orientation and cross section of GaN NWs growth with a judicial choice of substrate [36]. They synthesized [1 − 100] oriented GaN NWs with triangular cross section on (100) γ-$LiAlO_2$ substrate and [0001] oriented GaN NWs with hexagonal cross section on (111) MgO substrate [36]. The twofold symmetry of oxygen sublattice in the (100) plane of γ-$LiAlO_2$ matches with the twofold symmetry of the (100) plane of wurtzite GaN. On the other hand, the threefold symmetry of (111) plane of MgO matches with the threefold symmetry of (001) plane of GaN. He et al. synthesized [10 − 10] oriented GaN nanowires on (100) γ-$LiAlO_2$ substrate [37]. To demonstrate the substrate effect, they grew GaN nanowires on Si (100) substrate under the same experimental conditions and found that the nanowires in this case are irregular and randomly oriented on the substrate. Several groups have also used Si (111) substrate to grow vertical GaN and InN NWs because the atoms in Si (111) plane are arranged in a hexagonal array and the interatomic distance matches relative closely with the lattice constant of GaN [38–42]. Dayeh.et al. also reported the effect of V/III ratio and temperature on the growth rate and morphology of InAs nanowires grown on InAs(111)B substrate using organometallic vapor phase epitaxy method. They were able to control the NW morphology by tuning both the growth temperature and group III flow rate [43].

In this paper, we studied the synthesis of single crystal, wurtzite structured InN NWs on top of Si (100) substrate by CVD. Pure In and ammonia (NH_3) are used as precursors. We observed the mixture of ⟨10 − 10⟩ and ⟨0001⟩ oriented InN NWs grown on Si (100) substrate, which could be attributed to the lattice and crystal symmetry mismatch between InN and Si (100) substrate: (100) plane of Si has fourfold symmetry whereas (100) plane of wurtzite InN has twofold symmetry and (001) plane of wurtzite InN has threefold symmetry. The in-plane lattice constant of Si a=5.431 Å does not match well with the lattice constant of InN (a=3.545 Å). Though the material synthesis for device applications is mainly based on MBE or MOCVD currently, NWs grown via VLS growth mechanism does not necessarily to be performed in MBE or MOCVD. The CVD technique has some unique features such as simple, low cost and scalability which make it attractive.

2. Experimental section

Fig. 1 shows the schematic of the horizontal CVD system with 2 in. tube diameter used for InN NWs growth. A three-zone tube furnace with separate temperature controller for each zone was used for the synthesis of the InN NWs. Prior the CVD growth, (100) Si substrate was soaked in 10% HF for 90 s, rinsed by de-ionized water and dried with nitrogen flow. Au film with 15 Å thickness was deposited on top of the substrate via thermal evaporation.

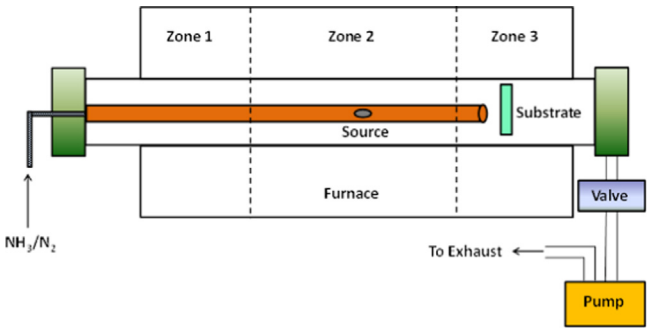

Fig. 1. Schematic diagram of the three-zone furnace chamber for InN nanowire growth.

High purity indium foil (Alfa Aesar, 99.998%) serving as group III precursor, was placed in an alumina crucible. The crucible was kept inside an inner quartz tube. The Si substrate was placed vertically at the downstream of the tube separated from the indium source by 4 in. The source was kept at zone 2 and the substrate was kept at zone 3 inside the chamber. Prior to heating up the chamber to the desired growth temperature, the chamber was pumped down to a base pressure of 10^{-4} Torr. Then it was purged with nitrogen (500 sccm) for 30 min. The zone 2 temperature was set at 670 °C to decompose the NH_3 molecules and the zone 3 temperature was set at 580 °C to assist the growth of InN NWs on Si substrate. Upon reaching the desired temperature, the growth was carried out by introducing ammonia inside the chamber at a flow rate of 500 sccm. Note that the dissociation rate of NH_3 depends on temperature, pressure and the catalyst being used. As the temperature increases and the pressure decreases, the decomposition rate increases. The complete decomposition of NH_3 to N_2 and H_2 occurs at ~430 °C at atmospheric pressure [44]. The growth time was 1.5 h and the growth pressure was ~10 Torr. To prevent the decomposition of InN, NH_3 was continued to flow during cool down until the temperature went down to 400 °C, similar to the reported references [17,18,21]. Then N_2 was flown and the sample was taken out after cooling down to room temperature.

The structure, morphology and composition of the InN NWs were characterized by using X-ray diffraction (XRD), scanning electron microscopy (SEM), field emission scanning electron microscopy (FESEM) and transmission electron microscopy (TEM). XRD spectra were collected on a Bruker Discover D8 with Co Kα radiation (1.79026 Å). The X-ray beam diameter is 500 μm. SEM images were taken with Tescan Vega-3 SBH, with electron beam voltage of 3 kV. FESEM images were taken with Helios 650, with electron beam voltage of 2 kV. High resolution transmission electron microscopy (HRTEM) images, energy dispersive spectroscopy (EDS) and selected-area electron diffraction (SAED) were taken with FEI Tecnai F30 at 300 kV. For the preparation of the TEM sample, the InN NWs were first dispersed in ethanol and then transferred to a Cu grid covered with carbon film.

3. Results and discussion

Fig. 2 shows the XRD spectra of the InN NWs. The diffraction peaks match perfectly with wurtzite InN which suggests the growth of high quality InN material. Based on the 2θ data of the (100) and (002) peaks, the lattice parameters are a=3.536 Å and c=5.709 Å (33.967° and 36.524° for (100) and (002) planes, respectively), which are in good agreement with bulk InN lattice parameters of a=3.545 Å and c=5.703 Å. The (100) and (002) planes in the diffraction spectra correspond to ⟨10 − 10⟩ and ⟨0001⟩ oriented NWs respectively. The (101) plane is a second order glide plane responsible for prismatic stacking fault (PSF) [41].

The 60° tilted SEM images of the InN NWs grown on Au coated Si (100) substrate are shown in Fig. 3. From Fig. 3(a), high density tilted InN NWs were grown on Si substrate. Fig. 3(b) shows the FESEM image of the InN NWs. As can be seen from Fig. 3(b)–(d), the nanowires consist of both triangular and hexagonal cross sections. The diameter of the InN NWs reduces as the NWs grow longer. The NWs with hexagonal cross section have an average diameter span of ~22 nm at the tip and ~260 nm at the bottom and lengths ranges between 2–2.5 μm, which indicates an average growth rate of 1.3–1.7 μm/h. On the other hand, the NWs with triangular cross section have an average diameter span of ~55 nm and have an average length of ~1.3 μm which indicates an average growth rate of 0.9 μm/h. The NWs with hexagonal cross section have a higher growth rate than those with triangular cross section. Based on a general mass transport model, the growth rate of NW depends on the diameter of the NW [45]. With NW diameter ranges between 20–100 nm, thinner wires grow faster than thicker ones. This model explains our observation of the higher growth rate of the thinner InN NWs with hexagonal cross section than the one with triangular cross section. There is a wide range of the reported InN NW diameter from literature: Tang et al. reported a growth rate of 4–10 μm/h for their InN NWs grown using Au nanoparticles [23]; Liang et al. synthesized InN NWs with diameter of 40–80 nm and length up to 5 μm on Au patterned Si substrate and had a growth rate of ~0.6 μm/h [24]. The growth rate of NWs depends on multiple factors including NW diameter, growth pressure, supersaturation etc. Typically, the NW growth rate is much faster than that of the corresponding thin film growth. Note that the growth rate of InN thin films is much slower (0.01–0.4 μm/h) by using MOVPE [14]. Due to the high density of the grown InN NWs, it is challenging to statistically count the percentage of the m-plane and c-plane InN NWs. Here, based on the SEM image with dimension of $3 \times 3\ \mu m^2$, the ratio of the InN NWs with triangular cross section to that of the ones with hexagonal cross section is about 2:3.

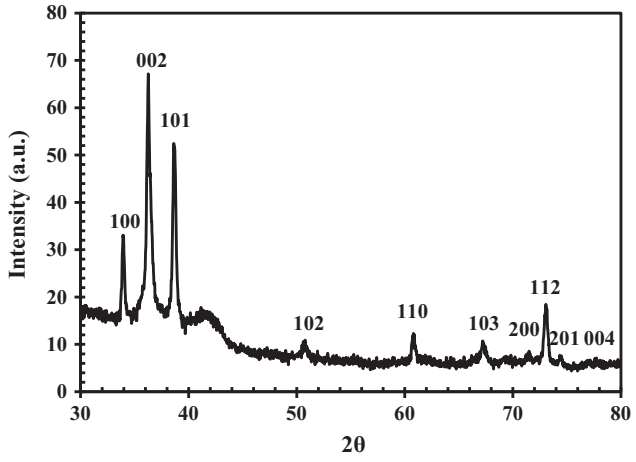

Fig. 2. XRD spectrum of InN NWs. The InN NWs are consisted of wurtzite crystal structure. The corresponding indices are marked above the respective diffraction peaks.

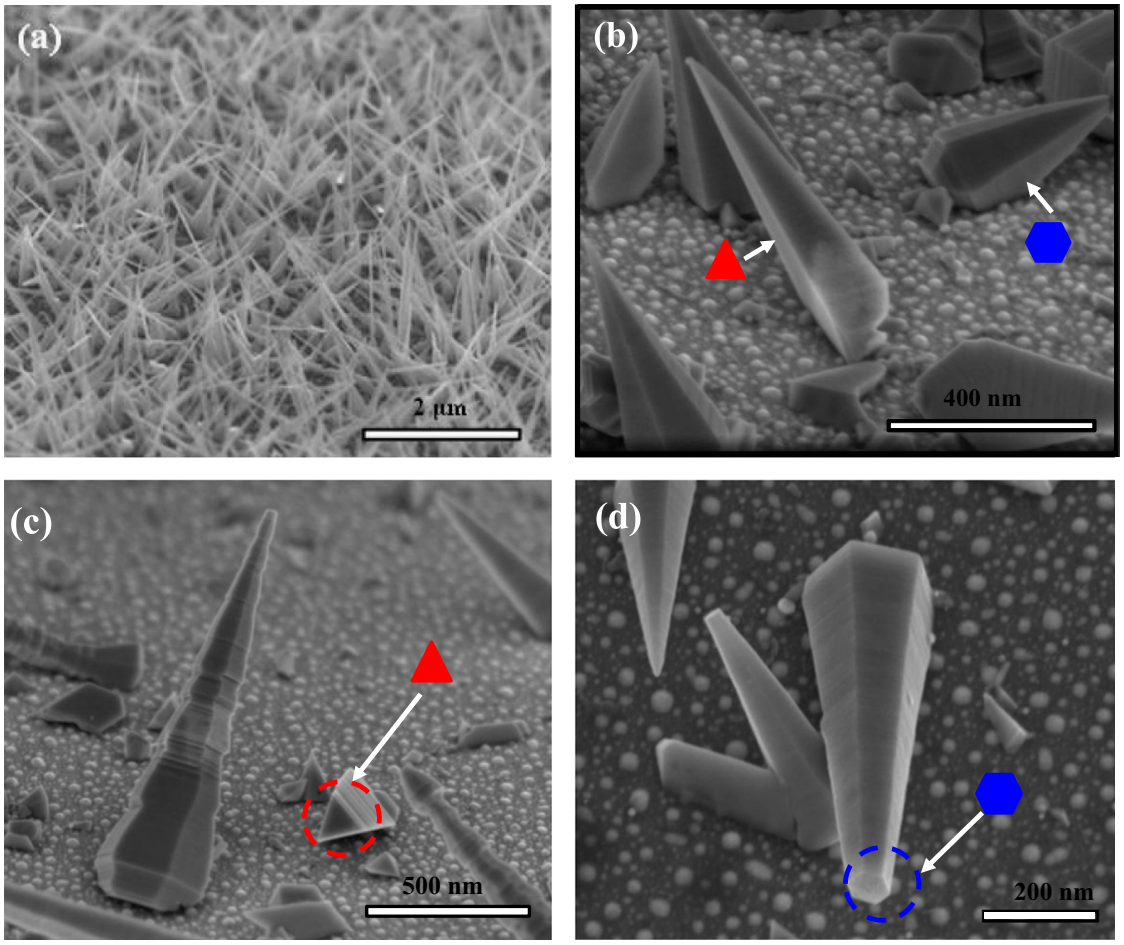

Fig. 3. (a) SEM image of InN NWs viewed at 60° from the surface normal. (b–d) FESEM images of InN NWs. The nanowires have triangular [marked with red triangle in (b) and (c)] and hexagonal [marked with blue hexagon in (b) and (d)] cross sections. (For interpretation of the references to color in this figure legend, the reader is referred to the web version of this article.)

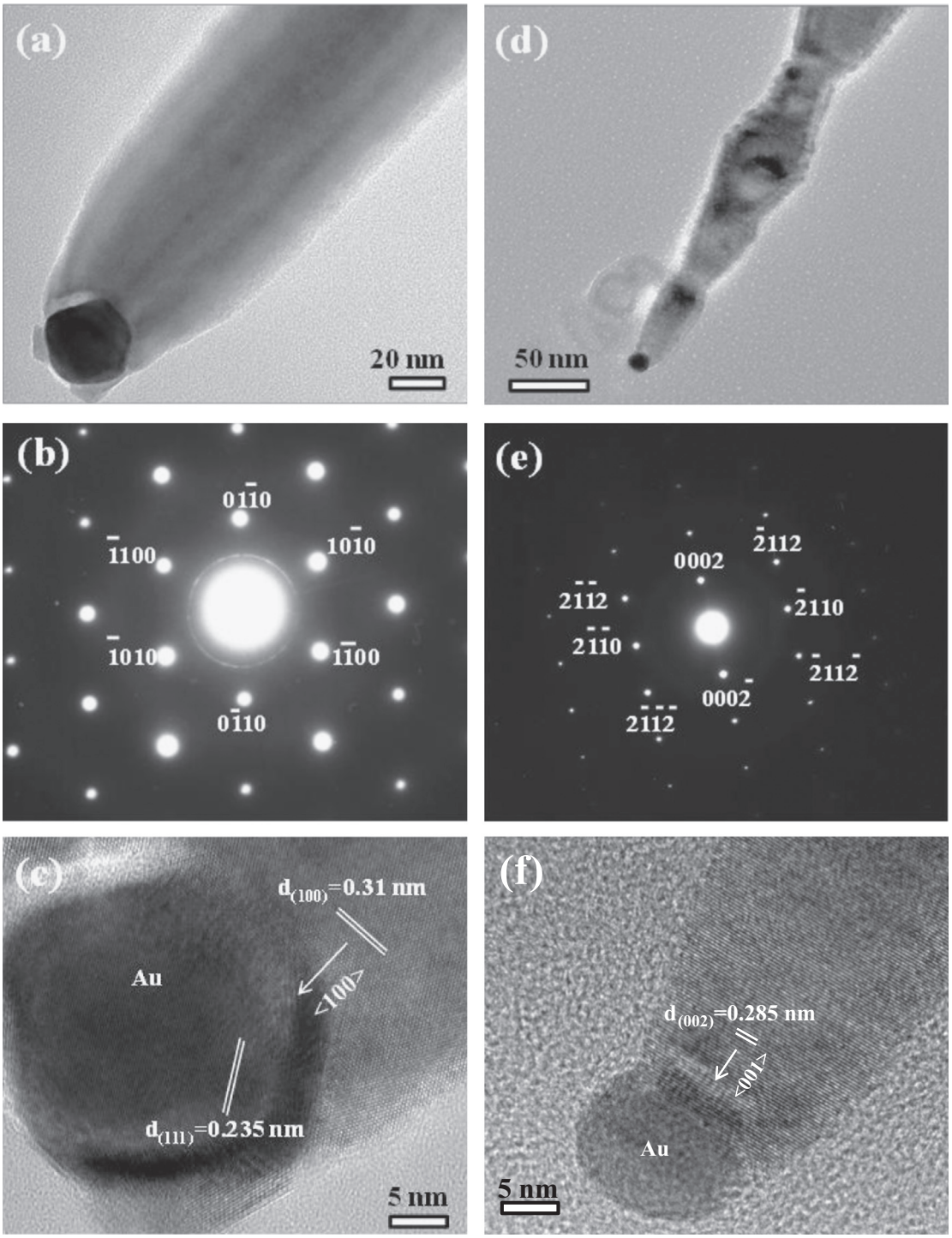

Fig. 4. (a, d) TEM images of m-plane and c-plane InN NWs taken at the tip; (b, e) SAED patterns of the m-plane and c-plane InN NWs taken along the [0001] and [01 – 10] zone axis, respectively; (c, f) HRTEM lattice images of m-plane and c-plane InN NWs taken at the interface between an Au nanoparticle and the InN NW.

TEM images of InN NWs with triangular and hexagonal cross sections are shown in Fig. 4(a) and (d). An Au particle is clearly visible at the tip of the NWs in both cases which confirms that the growth of the InN NWs was based on VLS growth mechanism. The side walls of the NWs with hexagonal cross section are faceted whereas the side walls of the NWs with triangular cross section are smooth. This indicates the growth of NWs with triangular cross section is more stable than the growth of the NWs with hexagonal cross section. We assume that the faceting of the side walls of the NWs are due to the instability of the catalyst droplet during the growth. Since the diameters of the nanowires grown via VLS mechanism are determined by the catalyst size [46], oscillation of the catalyst during growth could lead to the faceting of the side walls of the InN NWs. It has been reported previously that the oversupply of source vapor and interplay of surface energies of the wire and the liquid droplet make the catalyst unstable during growth and this leads to the formation of sawtooth faceted side walls of ZnO [47] and Si nanowires [48]. Based on these studies, we assume that for the InN NWs grown along the polar orientation, the Au droplet is unstable with higher surface energy. This needs further studies to confirm. Fig. 4(b) and (e) shows the selected area SAED patterns of the NWs taken along the [0001] and [01 – 10] zone axis,

respectively. The patterns were taken at the body of the NWs. Different SAED patterns were taken at different positions along the NWs and similar diffraction patterns were observed (not shown). The SAED pattern confirms that the synthesized materials are single crystalline wurtzite InN. The HRTEM images (Fig. 4(c) and (f)) taken at the interface between Au particle and InN NW clearly shows the lattice fringes. From Fig. 4(c), the interplanar spacing measured at the Au particle is 0.235 nm, corresponding to Au (111) plane. The interplanar spacing measured for InN NWs with triangular cross section is 0.31 nm, which corresponds to wurtzite InN (100) plane. Also (100) plane of InN is perpendicular to the NW growth direction which indicates that the NWs grew along the ⟨10−10⟩ m-plane direction. On the other hand, the interplanar spacing measured for InN NWs with hexagonal cross section is 0.285 nm, which corresponds to wurtzite InN (002) plane. The (002) plane of InN is perpendicular to the NW growth direction which indicates that the NWs grew along the ⟨0001⟩ c-plane direction. Our result matches well with other reports where people have seen polar and non-polar GaN NWs with hexagonal and triangular cross sections respectively [36]. The m-plane NWs are enclosed by (001), (112) and (−1−12) side planes and the c-plane NWs are enclosed by {100} side planes.

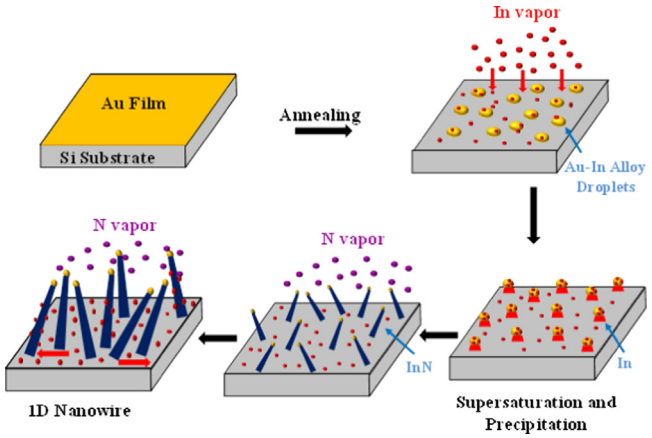

Fig. 5. Schematic of InN nanowire synthesis process, which indicates the proposed growth mechanism.

The presence of an Au particle at the nanowire tip in the TEM image confirmed that the InN NWs were grown based on the VLS mechanism. Au clusters on Si substrate acted as the nucleation centers. Indium vapor generated from the starting material was adsorbed on the Au clusters due to the selective wetting of indium on Au than on the substrate material. The diffusion of these indium atoms into the Au clusters led to the formation of Au/In alloy droplets. The subsequent In flux then supersaturated the droplets and nucleation of the indium phase occurred. The N atoms generated from the dissociation of NH_3 then reacted with the indium atoms precipitated out of the Au/In alloy droplets and led to the InN NW growth. The grown NWs are tapered with larger

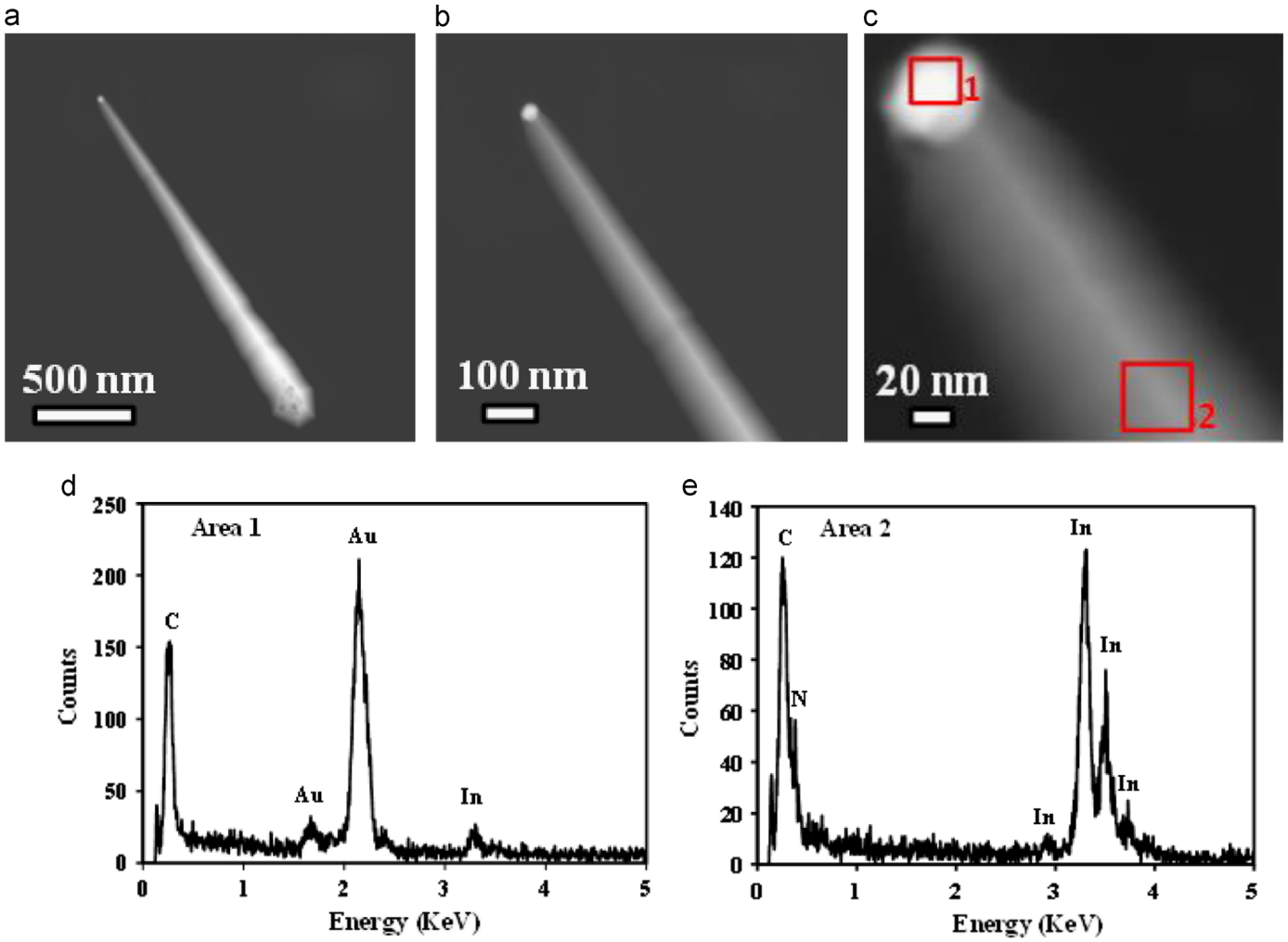

Fig. 6. (a)–(c) STEM images of a single InN NW at different magnifications. EDS spectrum of (d) Au nanoparticle (area 1), and (e) nanowire stem (area 2). The corresponding areas are marked in (c). Note that the carbon signal is generated from the TEM grid.

diameter at the bottom and smaller diameter at the top. The tapered NW growth can possibly be explained by two mechanisms: (1) the reduction of Au particle size during the NW growth due to the Au wetting of the NW side walls; and (2) the simultaneous vertical and lateral growth of NWs. The phenomenon of surface migration of gold on the growths of silicon NWs has been observed experimentally [49]. Au migrates through the surface from small catalyst droplet to large catalyst droplet to reduce the total droplet surface area. Part of the Au could wet the NW side walls. Thus, there is a gradual decrease in catalyst size during growth which leads to the formation of tapered nanowire. In addition, as illustrated in Fig. 5, the Au particles are known to serve as a sink for the precursor vapors. There exists a supersaturation gradient along the wire [50]. The supersaturation is the lowest at the Au-nanowire interface. As the In-vapor deposited on top of the Si substrate accumulates, part of the indium atoms diffuse through the substrate to the NWs and nucleation occurs on the side facets of the NWs. Since the NW bases are grown first and they are located at a close proximity to the substrate, they receive greater portion of the precursor material diffusing through the substrate than the nanowire tip and have higher lateral growth rate [51]. We believe the surface diffusion is the dominant mechanism for the tapered nanowire growth since ~80% of the group III precursor comes from diffusing species and ~20% comes from direct impingement on catalyst during nanowire growth [52].

Fig. 6 shows the STEM images of a single m-plane InN NW. Fig. 6(d) and (e) show the EDS taken at the tip (area 1) and the body (area 2) of a single InN NW. It can be seen that the tip is primarily consisted of Au, and with small amount of In. The body of the NW is consisted of In and N. Quantitative analysis reveals that the In/N atomic ratio at the body of the nanowire is 48.98:50.81. Note that the N peak overlaps with the carbon peak. And the carbon signal comes from the TEM grid.

4. Conclusion

In conclusion, we have observed the mixture of both nonpolar m-plane and polar c-plane InN NWs grown on Si (100) substrate via chemical vapor deposition approach. XRD, SAED and HRTEM data show that the synthesized InN NWs are of high quality and have a single crystalline wurtzite structure. The mixture of the two different orientations of the NWs were due to lattice and crystal symmetry mismatch between InN and Si (100) substrate. InN NWs grown along the nonpolar m-plane with triangular cross section show smooth side wall morphology, while those grown along the polar c-plane with hexagonal cross section show faceted side wall morphology. Although no direct application with the grown mixture of InN NWs at the current stage, the studies in the manuscript provide a new finding that potentially will advance future research to control the growth of InN NWs. Further studies on the relationship among substrate orientation, catalyst stability and NW orientation are necessary. Synthesis of InN NWs in large quantity and better uniformity will enable us to investigate their intrinsic properties for potential application in future nanoscale electronic and optoelectronic devices.

Acknowledgments

The authors acknowledge financial support through start-up funds from Case Western Reserve University. Part of the material characterizations were performed at the Swagelok Center for Surface Analysis of Materials (SCSAM) at CWRU.

References

[1] Y. Uemoto, M. Hikita, H. Ueno, H. Matsuo, H. Ishida, M. Yanagihara, T. Ueda, T. Tanaka, D. Ueda, IEEE Trans. Electron Devices 54 (2007) 3393.
[2] S. Nakamura, M. Senoh, N. Iwasa, S. Nagahama, Jpn. J. Appl. Phys. 34 (1995) L797.
[3] M.H. Crawford, IEEE J. Sel. Topic Quantum Electron. 15 (2009) 1028.
[4] J.J. Wierer, A. David, M.M. Megens, Nat. Photonics 3 (2009) 163.
[5] S. Nakamura, M. Senoh, S. Nagahama, N. Iwasa, T. Yamada, T. Matsushita, H. Kiyoku, Y. Sugimoto, Jpn. J. Appl. Phys. 35 (1996) L74.
[6] S. Gradečak, F. Qian, Y. Li, H.-G. Park, C.M. Lieber, Appl. Phys. Lett. 87 (2005) 173111.
[7] H. Yoshida, Y. Yamashita, M. Kuwabara, H. Kan, Nat. Photonics 2 (2008) 551.
[8] J. Wu, W. Walukiewicz, K.M. Yu, J.W. Ager III, E.E. Haller, H. Lu, W.J. Schaff, Y. Saito, Y. Nanishi, Appl. Phys. Lett. 80 (2002) 3967.
[9] M. Jamil, H. Zhao, J.B. Higgins, N. Tansu, Phys. Status Solidi A 205 (2008) 2886.
[10] B.E. Foutz, S.K. O'Leary, M.S. Shur, L.F. Eastman, J. Appl. Phys. 85 (1999) 7727.
[11] V.W.L. Chin, T.L. Tansley, T. Osotchan, J. Appl. Phys. 75 (1994) 7365.
[12] B.R. Nag, J. Cryst. Growth 35 (2004) 269.
[13] Y. Huang, H. Wang, Q. Sun, J. Chen, D.Y. Li, Y.T. Wang, H. Yang, J. Cryst. Growth 13 (2005) 276.
[14] B. Maleyre, S. Ruffenach, O. Briot, B. Gil, A. Van der Lee, Superlattices Microstruct. 36 (2004) 517.
[15] R. Walther, D. Litvinov, M. Fotouhi, R. Schneider, D. Gerthsen, R. Vohringer, D.Z. Hu, D.M. Schaadt, J. Cryst. Growth 340 (2012) 1.
[16] J. Zhang, L. Zhang, X. Peng, X. Wang, J. Mater. Chem. 12 (2002) 802.
[17] M.C. Johnson, C.J. Lee, E.D. Bourret-Courchesne, S.L. Konsek, S. Aloni, W.Q. Han, A. Zettl, Appl. Phys. Lett. 85 (2004) 5670.
[18] H.Y. Xu, Z. Liu, X.T. Zhang, S.K. Hark, Appl. Phys. Lett. 90 (2007) 113105.
[19] L. Yin, Y. Bando, D. Golberg, M. Li, Adv. Mater. 16 (2004) 1833.
[20] S. Luo, W. Zhou, Z. Zhang, L. Liu, X. Dou, J. Wang, X. Zhao, D. Liu, Y. Gao, L. Song, Y. Xiang, J. Zhou, S. Xie, Small 1 (2005) 1004.
[21] Guosheng Cheng, Eric Stern, Daniel Turner-Evans, Mark A Reed, Appl. Phys. Lett. 87 (2005) 253103.
[22] B. Schwenzer, L. Loeffler, R. Seshadri, S. Keller, F.F. Lange, S.P. DenBaars, U.K. Mishra, J. Mater. Chem. 14 (2004) 637.
[23] T. Tang, S. Han, W. Jin, X. Liu, C. Li, D. Zhang, C. Zhou, B. Chen, J. Han, M. Meyyapan, J. Mater. Res. 19 (2004) 423.
[24] C.H. Liang, L.C. Chen, J.S. Hwang, K.H. Chen, Y.T. Hung, Y.F. Chen, Appl. Phys. Lett. 81 (2002) 22.
[25] H. Liu, G. Cheng, Appl. Phys. Express 4 (2011) 105002.
[26] Z. Cai, S. Garzon, M.V.S. Chandrashekhar, R.A. Webb, G. Koley, J. Electronic Mater. 37 (2008) 5.
[27] Y. Yang, Y. Ling, G. Wang, X. Lu, Y. Tong, Y. Li, Nanoscale 5 (2013) 1820.
[28] S.K. Lim, S. Crawford, G. Haberfehlner, S. Gradečak, Nano Lett. 13 (2013) 331.
[29] M. He, S.N. Mohammad, J. Vac. Sci. Technol. B 25 (2007) 940.
[30] S. Vaddiraju, A. Mohite, A. Chin, M. Meyyappan, G. Sumanasekera, B.W. Alphenaar, M.K. Sunkara, Nano Lett. 5 (2005) 1625.
[31] K. Sardar, F.L. Deepak, A. Govindaraj, M.M. Seikh, C.N. Rao, Small 1 (2005) 91.
[32] Y.L. Chang, F. Li, A. Fatehi, Z. Mi, Nanotechnology 20 (2009) 345203.
[33] M. Yoshimoto, H. Yamamoto, W. Huang, H. Harima, J. Saraie, A. Chayahara, Y. Horino, Appl. Phys. Lett. 83 (2003) 3480.
[34] A.G. Bhuiyan, K. Sugita, K. Kasashima, A. Hashimoto, A. Yamamoto, V.Yu. Davydov, Appl. Phys. Lett. 83 (2003) 4788.
[35] S.A. Fortuna, X. Li, Semicond. Sci. Technol. 25 (2010) 024005.
[36] T. Kuykendall, P.J. Pauzauskie, Y. Zhang, J. Goldberger, D. Sirbuly, J. Denlinger, P. Yang, Nat. Mater. 3 (2004) 524.
[37] X. He, G. Meng, X. Zhu, M. Kong, Nano Res. 2 (2009) 321.
[38] M. Tchernycheva, C. Sartel, G. Cirlin, L. Travers, G. Patriarche, J.C. Harmand, L.S. Dang, J. Renards, B. Gayral, L. Nevou, F. Julien, Nanotechnology 18 (2007) 385306.
[39] D. Salomon, A. Dussaigne, M. Lafossas, C. Durand, C. Bougerol, P. Ferret, J. Eymery, Nanoscale Res. Lett. 8 (2013) 61.
[40] R. Calarco, R.J. Meijers, R.K. Debnath, T. Stoica, E. Sutter, H. Luth, Nano Lett. 7 (2007) 2248.
[41] Y.B. Tang, Z.H. Chen, H.S. Song, C.S. Lee, H.T. Cong, H.M. Cheng, W.J. Zhang, I. Bello, S.T. Lee, Nano Lett. 8 (2008) 4191.
[42] J.E. Northrup, Appl. Phys. Lett. 72 (1998) 2316.
[43] S.A. Dayeh, E.T. Yu, D. Wang, Nano Lett. 7 (2007) 2486.
[44] V. Hacker, K. Kordesch, Handbook of Fuel Cells – Fundamentals, Technology and Applications, John Wiley & Sons, Ltd, Chichester (2003) 121.
[45] J. Johansson, B.A. Wacaser, K.A. Dick, W. Seifert, Nanotechnology 17 (2006) S355.
[46] Y. Cui, L.J. Lauhon, M.S. Gudiksen, J. Wang, C.M. Lieber, Appl. Phys. Lett. 78 (2001) 2214.
[47] A. Kar, K.B. Low, M. Oye, M.A. Stroscio, M. Dutta, A. Nicholls, M. Meyyappan, Nanoscale Res. Lett. 6 (2011) 3.
[48] F.M. Ross, J. Tersoff, M.C. Reuter, Phys. Rev. Lett. 95 (2005) 146104.
[49] J.B. Hannon, S. Kodambaka, F.M. Ross, R.M. Tromp, Nature 440 (2006) 69.
[50] K.A. Dick, K. Deppert, T. Mårtensson, B. Mandl, L. Samuelson, W. Seifert, Nano Lett. 5 (2005) 761.
[51] H.J. Joyce, Q. Gao, H.H. Tan, C. Jagadish, Y. Kim, J. Zou, L.M. Smith, H.E. Jackson, J.M.Y. Rice, P. Parkinson, M.B. Johnston, Prog. Quantum Electron. 35 (2011) 23.
[52] L.E. Jensen, M.T. Bjork, S. Jeppesen, A.I. Persson, B.J. Ohlsson, L. Samuelson, Nano Lett. 4 (2004) 1961.